


Disassembling infra-low-frequency neurofeedback: A neurophysiological investigation of its feedback components

Nuno M.P. de Matos^a, Philipp Stämpfli^a, Erich Seifritz^b, Mike Brügger^{a,*} 

^a Magnetic Resonance Center of the University Hospital of Psychiatry Zurich and University of Zurich, Zurich, Switzerland

^b Department of Adult Psychiatry and Psychotherapy, Psychiatric University Clinic Zurich and University of Zurich, Zurich, Switzerland

ARTICLE INFO

Keywords:

Classic Frequency Band
 Infra-Low-Frequency Neurofeedback
 Multivariate approach incorporating fMRI
 EEG, Respiration, Electrodermal Activity
 HRV, Questionnaires
 Functional connectivity Multivariate Pattern
 Analysis (fc-MVPA)
 Seed-to-Voxel Analysis

ABSTRACT

Infra-Low-Frequency Neurofeedback (ILF-NFB), an EEG-based intervention, integrates specific electrode placements with “classic” frequency band (FB; 1–35 Hz) and infra-low-frequency (ILF; <0.1 Hz) components. Despite increasing clinical use, systematic studies of their individual and combined effects on neurophysiology remain limited. To address this gap, we conducted three randomized, sham-controlled, double-blind crossover studies (each with 40 healthy volunteers) examining FB-Only (Study 1), ILF-Only (Study 2), and combined FB&ILF (Study 3) protocols. The primary outcome was a functional connectivity multivariate pattern analysis (fc-MVPA) of resting-state fMRI data, using false discovery rate (FDR)-corrected thresholds ($p < 0.05$) at voxel and cluster levels. Exploratory analyses included post-hoc seed-to-voxel analyses (Bonferroni-corrected, $p\text{-FWE} < 0.0083$), psychophysiological measures (heart rate variability [HRV], respiration), and neurofeedback state questionnaires.

For FB-Only and ILF-Only, fc-MVPA interaction effects did not survive FDR correction. For study with combined FB&ILF, fc-MVPA revealed significant interaction effects ([Post-Pre Verum] vs. [Post-Pre Sham]), identifying clusters in parietal, occipital, and cingulate regions. Post-hoc seed-to-voxel analyses using the fc-MVPA clusters as seeds suggested that FB&ILF increased connectivity between posterior midline/parieto-occipital regions and the right dorsolateral prefrontal cortex; no significant changes were observed in sham conditions.

HRV showed a significant interaction effect only in the FB&ILF study. Questionnaires revealed greater perceived controllability and signal causation in Verum vs. Sham for FB-Only and FB&ILF, but not ILF-Only. Verum ILF-Only improved concentration and well-being, though participants also reported increased nervousness and sleepiness post-session.

Overall, our findings indicate that the combined FB&ILF application induces robust connectivity and autonomic changes, providing initial evidence to support clinical ILF-NFB effects and warranting further mechanistic studies.

1. Introduction

Neurofeedback (NFB) is a branch of biofeedback in which brain-derived signals are analyzed in real-time and presented back to the individual as visual, auditory, or haptic feedback. The primary aim of NFB is to enable self-regulation of neural activity, which may support clinical treatments for neurological and psychiatric conditions or serve as a neuroenhancement tool (Enriquez-Geppert et al. 2017; Marzbani et al. 2016). Various neuroimaging modalities have been utilized for NFB, including functional magnetic resonance imaging (fMRI) and near-infrared spectroscopy (fNIRS) for hemodynamic measures, as well

as electrophysiology-based methods such as invasive electrocorticography (ECoG), magnetoencephalography (MEG), and the most commonly applied method, electroencephalography (EEG) (Sitaram et al. 2017).

The roots of EEG-based NFB interventions date back to the 1960s when early experiments demonstrated that animals and individuals could learn to modulate their brain activity through positive reinforcement learning (Kamiya 2011, Kamiya 1968; Sherlin et al. 2011; Sitaram et al. 2017; Wyrwicka und Serman 1968). From its inception, EEG-NFB training was designed to enable self-regulation by facilitating voluntary control over specific neural signals. Early approaches focused on

* Corresponding author.

E-mail address: mike.bruegger@bli.uzh.ch (M. Brügger).

<https://doi.org/10.1016/j.neuroimage.2025.121647>

Received 17 April 2025; Received in revised form 10 November 2025; Accepted 11 December 2025

Available online 12 December 2025

1053-8119/© 2025 Published by Elsevier Inc. This is an open access article under the CC BY-NC-ND license (<http://creativecommons.org/licenses/by-nc-nd/4.0/>).

modulating frequency bands, coherence between electrode sites, and slow cortical potentials. These signals continue to be widely used in EEG-NFB today, with frequency bands being the most commonly applied parameter (Omejc et al. 2019).

A typical EEG-NFB session involves the real-time isolation of a pre-selected neural signal, often the amplitude or coherence of a specific EEG frequency band, from ongoing brain activity. This signal is extracted via electrodes placed on the scalp, processed by dedicated software, and transformed into a simple visual or auditory feedback display. For example, the display might be a moving bar, a flame, or an animated object whose height, brightness, or speed reflects the moment-to-moment amplitude of the target frequency band. Participants are explicitly instructed to use mental strategies to alter this feedback in a desired direction (e.g., increase SMR amplitude or decrease theta amplitude) to achieve a reinforcement goal, such as making the bar rise or the flame grow. Positive reinforcement is typically provided when the signal meets the target criteria. Over repeated trials, this operant conditioning approach is intended to train volitional self-regulation of the targeted brain activity, with the feedback closely linked to the participant's ongoing neural state.

Studies applying EEG-NFB for self-regulation using the above mentioned types of signals report improvements in a wide range of clinical conditions (Kober et al. 2015; Marzbani et al. 2016; Renton et al. 2017; Sitaram et al. 2017; van der Kolk et al. 2016, 2019; Zuberer et al. 2015) and enhancement in cognitive and performance in healthy subjects (Cho et al. 2008; Engelbregt et al. 2016; Enriquez-Geppert et al. 2017; Hoedlmoser et al. 2008; Gruzeliier 2014a, 2014b)

1.1. Infra-low-frequency neurofeedback (ILF-NFB)

First applied by Othmer et al. in 2006, ILF-NFB emerged primarily from clinical observations and experimentation, and has since been further explored and optimized (Othmer 2020; Othmer et al. 2011, 2013).

This method differs substantially from other EEG-NFB techniques, particularly in its emphasis on very slow oscillations beyond the frequency range commonly targeted in explicit EEG-NFB paradigms (Bazzana et al. 2022; Haus et al. 2020; Othmer et al. 2013; Schmidt 2024). The most distinctive aspect of ILF-NFB concerns the extracted brain signals:

- Classic frequency band (FB): The first category consists of the combined signal of 8 frequency bands ranging from 1 to 35 Hz typically used in standard EEG-NFB.
- Infra-low frequency (ILF): The second category are infra-low-frequency signals with frequencies < 0.1 Hz, thought to reflect slow shifts in electrical potentials between the two targeted underlying brain regions.

ILF-NFB follows a symptom-driven approach, tailoring both electrode placement and training frequencies to individual needs. ILF-NFB employs bipolar electrode placements depending on clinical observations of patient symptoms. Similarly, ILF settings are dynamically adjusted to the participant's subjective responses, ensuring a flexible and personalized intervention (Haus et al. 2020; Othmer et al. 2013).

In contrast to the explicit, volitional self-regulation approach described above – thus the “typical” NFB approach - ILF-NFB follows an implicit training strategy. Rather than instructing participants to actively change the feedback signal in a particular direction, it emphasizes passive observation of feedback animations while both FB and ILF components are extracted and presented simultaneously. This represents a paradigm shift in neuromodulatory strategies, focusing on the brain's capacity for endogenous regulation without conscious strategy use.

Over the last decades, ILF-NFB has been the subject of various clinical investigations. Treatment efficacy has been reported in a broad range of medical conditions, including depression (Grin-Yatsenko et al.

2018), post-traumatic stress disorder (PTSD) (Gerge 2020), autism (Legarda et al. 2011), attention deficit and hyperactivity (Schneider et al. 2022), neurological (Carlson und Ross 2021) and eating disorders. For a comprehensive overview, readers are referred to Bazzana et al. (2022). While ILF-NFB shows promising results across a wide range of symptoms, Bazzana et al. (2022) emphasized that its therapeutic success may depend on its highly individualized, symptom-based approach, which requires close patient–therapist interaction for selecting electrode positions and determining optimal ILF settings.

Given the pronounced patient–therapist interactions, the variability in treatment dose (ranging from 4 to 40 sessions), and the limited characterization of ILF-NFB's neurophysiological mechanisms, an important question arises: To what extent are the observed clinical effects attributable to the protocol's specific signal components?

This question aligns with a recent consensus framework which distinguishes five sources of treatment-related change in NFB studies: (1) NFB-specific effects (target signal modulation), (2) NFB non-specific effects (feedback environment), (3) general non-specific effects (e.g., expectations, placebo), (4) repetition-related effects, and (5) natural effects such as spontaneous remission (Ros et al. 2020). Carefully designed non-clinical studies are essential to control for these factors and to isolate genuine neurofeedback-specific mechanisms.

So far, very few foundational studies have investigated the mechanisms of ILF-NFB. Among them, only one sham-controlled fMRI study (Dobrushina et al. 2020) demonstrated ILF-NFB-specific changes in large-scale connectivity across salience, language, and visual networks. However, this work focused on predefined ROIs, and the field still lacks a comprehensive, voxel-level understanding of how ILF and FB components contribute individually or in combination to neurophysiological effects. The present study addresses this gap.

1.2. Aim of the present work

In the present report, we propose a three-study approach to evaluate the specific effects of the classic frequency band (FB) and infra-low frequency (ILF) signal components on large-scale brain connectivity when applied separately and in combination. All three studies employed identical implicit neurofeedback protocols, differing only in the composition of the real-time EEG-derived feedback signal (FB only, ILF only, or FB&ILF).

This design addresses a key gap in the literature: while ILF-NFB has traditionally presented FB and ILF signals together based on clinical practice, the necessity of this simultaneous application has never been scientifically tested, either for clinical outcomes or for objectively measurable neurophysiological effects.

We designed the three studies in line with the consensus recommendations proposed by Ros et al. (2020) to reduce ambiguity as much as possible when examining NFB-specific effects. To this end, we conducted three randomized, sham-controlled, double-blind crossover studies, each with 40 complete datasets from healthy participants:

- Study 1 (FB-Only): FB training alone vs. sham FB
- Study 2 (ILF-Only): ILF training alone vs. sham ILF
- Study 3 (FB & ILF): Combined FB and ILF training vs. sham FB & ILF

The primary endpoint in all studies was the identification of brain regions showing significant alterations in whole-brain connectivity patterns, assessed with functional connectivity multivariate pattern analysis (fc-MVPA). fc-MVPA is a hypothesis-free, voxel-wise method that evaluates the multivariate connectivity profile of each voxel with the rest of the brain (Nieto-Castanon 2022). This approach is well suited to exploratory research in implicit ILF-NFB, where the specific neural substrates are not yet established, as it avoids the constraints of a priori region-of-interest (ROI) selection and can detect distributed effects across large-scale networks.

Given the established correspondence between EEG activity and the

BOLD signal (Britz et al. 2010; Murta et al. 2015; Scheeringa et al. 2011), EEG modulation via neurofeedback can plausibly alter the functional connectome as measured by fMRI. Consistent with this, Dobrushina et al. (2020) reported ILF-NFB-induced BOLD connectivity changes in healthy participants, supporting the use of fMRI connectivity as a sensitive endpoint for assessing FB, ILF, and combined FB&ILF protocols.

In our design, significant clusters from the fc-MVPA interaction contrast ([Post-Pre Verum] vs. [Post-Pre Sham]) represent the main neuroimaging outcome. To further interpret these clusters, we conducted post-hoc seed-to-voxel analyses, using each fc-MVPA cluster as a seed to map its connectivity with the rest of the brain. This two-step approach first localizes regions with altered connectivity profiles (fc-MVPA) and then characterizes their specific network-level connections (seed-to-voxel), linking robust whole-brain findings to interpretable large-scale network effects. In addition to the imaging outcomes, psychophysiological parameters and questionnaire data were collected to explore potential effects on subjective experience and physiological state.

2. Materials & methods

The study was preregistered on the clinicaltrials.gov database (NCT05711550).

2.1. Subjects

Participants were recruited via the mailing list of the Department of Psychology, University of Zurich, and through the “Marktplatz” online advertisement platform of the University of Zurich and the Swiss Federal Institute of Technology (ETH).

Inclusion criteria were:

1. Age \geq 18 years
2. Self-reported good health
3. Fluency in German (to ensure accurate questionnaire responses)

Exclusion criteria included:

1. MRI contraindications
2. Alcohol or drug consumption within 24 h prior to participation
3. Pre-existing neurological or psychiatric conditions
4. Regular medication intake

Eligibility was assessed using an online screening survey before enrollment.

For each study, the target sample size was 40 complete datasets for the primary endpoint analysis. Additional participants were recruited as needed to replace dropouts, resulting in final sample sizes of:

- Study 1: 44 participants (mean age = 29.61 ± 10.15 years; 59 % female)
- Study 2: 42 participants (mean age = 27.26 ± 8.31 years; 69 % female)
- Study 3: 45 participants (mean age = 26.04 ± 8.24 years; 60 % female)

Each participant completed two sessions, separated by at least two weeks, receiving either verum or sham neurofeedback in a counter-balanced sequence. Sequence allocation was randomized (see *Neurofeedback setup and protocol*).

Participants received 180 CHF for completing each study. In cases of early withdrawal, compensation was prorated at 30 CHF per hour of participation.

There was no overlap in participant samples across the three studies; each involved a distinct, independently recruited cohort.

2.1.1. Experimental procedures

All studies were conducted at the Magnetic Resonance Center of the University Hospital of Psychiatry, Zurich. Each measurement day consisted of four main blocks (Fig. 1): (1) Preparation, (2) pre-fMRI, (3) verum/sham neurofeedback (NFB), and (4) post-fMRI.

2.1.2. Preparation (≈ 30 min)

Participants received an overview of the procedures and provided written informed consent. They then completed digital versions of the SF-A/R, SF-B/R, BFI-60, and a self-developed neurofeedback state questionnaire (pre-NFB). Standard MR-compatible clothing was provided, and all jewelry or piercings were removed. Electrodes for ECG were prepared inside the MR scanner, and psychophysiological monitoring equipment was connected.

2.1.3. Pre-fMRI (≈ 30 min)

Baseline MRI and psychophysiology measurements were recorded before the NFB intervention. For each participant’s first session, a T1-weighted anatomical scan was acquired to support fMRI preprocessing; placing this scan at the start allowed participants to acclimate to the scanner environment. Functional MRI recordings were then performed according to the study protocol.

2.1.4. Neurofeedback block (≈ 30 min)

Participants left the MR scanner and were brought to a climate-controlled NFB room. Electrodes were prepared for psychophysiological and EEG recordings, followed by the verum or sham NFB protocol (see *Neurofeedback setup and protocol*). Immediately after the intervention, all recording equipment was removed, and participants completed the post-NFB version of the state questionnaire, assessing their subjective experience and perceived mental-state changes compared to the preparation phase.

2.1.5. Post-fMRI (≈ 30 min)

Post-intervention fMRI recordings were conducted to enable pre-post comparisons. Preparations for psychophysiological and MRI data acquisition matched those of the pre-fMRI block.

Note: Questionnaire data other than the neurofeedback state questionnaire, as well as psychophysiological signals recorded during NFB (respiration, electrodermal activity, and heart-rate variability), will be analyzed and reported in future publications.

2.1.6. Neurofeedback setup and protocol

All neurofeedback (NFB) sessions were conducted in a dedicated, climate-controlled room. Participants were seated ~ 1.5 m from a 65” screen (16:9 aspect ratio) displaying the real-time feedback animation. EEG was recorded using a PAMEL Comby EEG cap with 34 sintered Ag/AgCl electrodes arranged according to the international 10–20 system. A full 31-channel ear-referential EEG recording was acquired in real time for verum conditions or replayed from a prerecorded dataset for sham conditions. This setup preserved the ability to perform future offline analyses while ensuring participants could not determine which channels contributed to feedback. Skin preparation involved gentle abrasion and conductive gel to keep impedances below 7 k Ω . Additional sensors recorded respiration (chest belt), electrodermal activity (electrodes on the medial phalanges of the left hand’s ring and middle finger), and heart rate variability (ECG).

2.1.7. Signal acquisition and processing

Full-band EEG was sampled at 256 Hz and processed in real time using Cygnet® neurofeedback software v.2.0.8.5 (BeeMedic GmbH, Singen, Germany) with a NeuroAmp® X39 amplifier. The software used was the standard commercial version with additional study-specific functions essential for double-blind conduction: (1) random allocation of participants to intervention sequences (verum–sham or sham–verum) without experimenter influence; (2) a sham module that replayed pre-

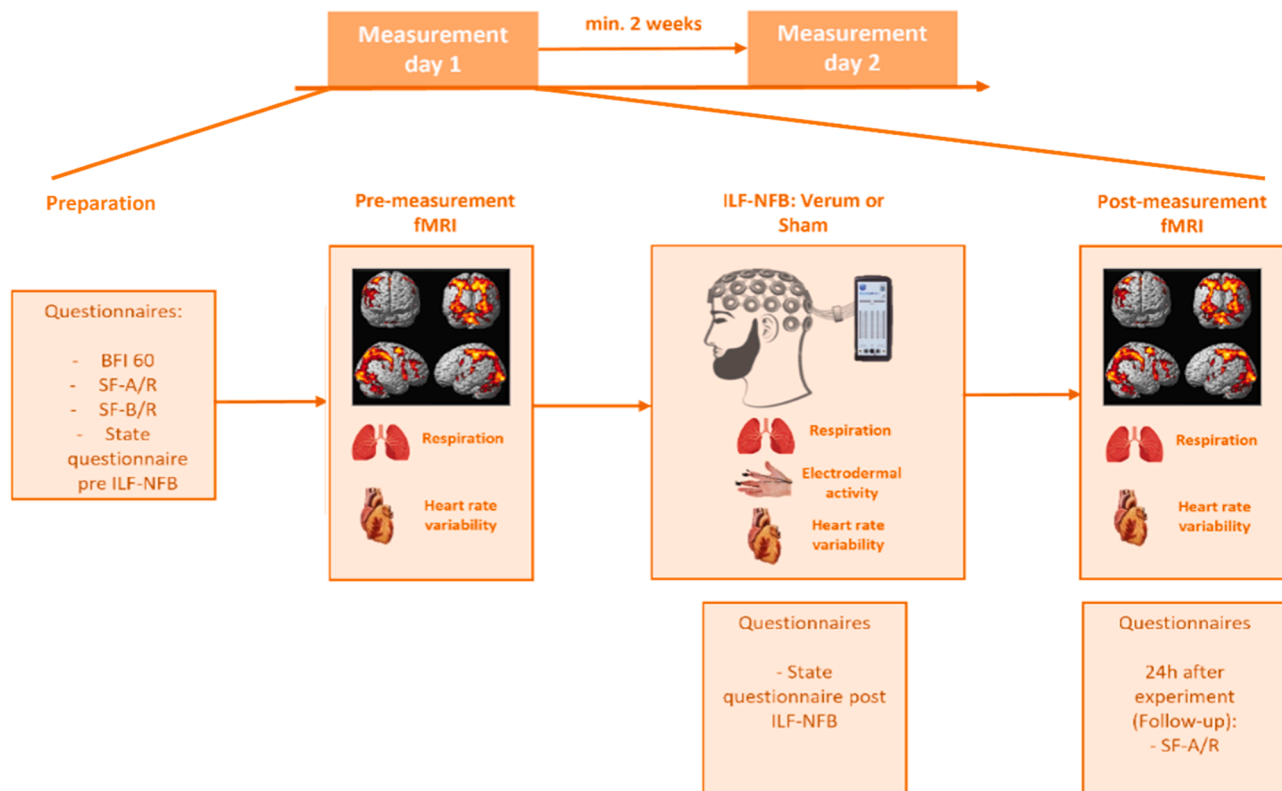


Fig. 1. Illustration of the experimental procedures performed at each measurement day. They were divided into four blocks: Preparation, pre-fMRI, ILF-NFB (verum or sham) and post-fMRI. The experimental procedures were identical for the three studies FB-Only, ILF-Only and FB&ILF.

recorded EEG data, collected with the same hardware and setup, while still analyzing the real EEG in parallel to detect muscular and movement artifacts, allowing artifact data to be integrated into the sham feedback to maintain blinding; and (3) an option to enable independent or combined presentation of the FB and ILF feedback components.

The neurofeedback protocol was based on a two-channel bipolar derivation reconstructed from the 31-channel recording at electrodes T4, P4, and Cz as reference.

The feedback animation “Dreamscapes – Wilderness” was chosen for its high tolerability, depicting a slow journey through a wooded, hilly landscape. The animation was accompanied by music. The Cygnet software computed two independent feedback components which modulated aspects of the animated imagery and music loudness:

1. FB component: The sum signal of the channels T4 + P4 was used. The frequency power amplitudes from eight frequency bands were extracted: Delta (2–5 Hz), Theta (5–8 Hz), Alpha (8–12 Hz), SMR (12–15 Hz), Beta (15–18 Hz), MidBeta (18–22), HiBeta (22–30 Hz), and LowGamma (30–40 Hz). For each band, an adaptive threshold was set to encompass 95 % of the current range of frequency power fluctuations, continuously adjusting so that the signal stayed within this range most of the time. This ensured that the presented feedback covered nearly the full spectrum of ongoing variations. The average distance from each band’s signal to its threshold was then used to modulate music volume and ambient fog.
2. ILF component: The difference signal $(T4-Cz) - (P4-Cz) = T4 - P4$ was low-pass filtered at 0.0001 mHz to capture infra-slow cortical potential shifts. The total power of this low-passed signal controlled movement speed, brightness, and color saturation of the animation.

All three protocols (FB-Only, ILF-Only, and FB&ILF) used an *implicit* design, with participants instructed immediately after component description to passively observe the animation without attempting to

control it. No explicit performance targets or reinforcement cues were provided. Depending on the study, feedback consisted of the FB component only (Study 1; fog and music volume), the ILF component only (Study 2; movement speed, brightness, and color saturation), or both components simultaneously (Study 3; fog and music volume reflecting FB activity; movement speed, brightness, color saturation reflecting ILF activity. All presented simultaneously).

Each NFB block lasted 30 min. After the session, electrodes were removed, and participants completed the post-NFB state questionnaire.

2.2. MRI data acquisition

Imaging data were acquired on a Philips Achieva 3T scanner (Philips Medical Systems, Best, The Netherlands), upgraded to the dStream platform, using a 32-channel receive-only head coil.

T1-weighted data were acquired with a 3D-T1w-TFE (Turbo-Field-Echo) sequence with following parameters: 160 sagittal slices, repetition time (TR) = 9.3 ms, echo time (TE) = 4.6 ms, acquisition voxel size = $1.0 \times 1.0 \times 1.0 \text{ mm}^3$, flip angle = 8° , FOV = $240 \times 240 \times 160 \text{ mm}^3$, turbo field echo factor: 120, scan duration 3 min 44 s.

Resting-state fMRI data was recorded using a T2*-weighted multi-band echo planar imaging (EPI) sequence containing 600 scans preceded by 5 discarded dummy scans with following parameters: 54 axial slices, TR = 1800 ms, TE = 30 ms, in-plane acquisition voxel size = $3.00 \times 3.00 \text{ mm}^2$, slice thickness = 3.0 mm, flip angle = 78° , field of view (FOV) = $220 \times 129.6 \times 220 \text{ mm}^3$, acquisition and reconstruction matrix = 128×128 , SENSE = 1.8, multiband factor = 3, slice gap = 0 mm. Slices were acquired in Philips-specific interleaved order. Total acquisition time: Approx. 18 min per session.

2.3. fMRI preprocessing and denoising

Analyses of fMRI data were performed using CONN (RRID:

SCR_009550) release 22.v2407 and SPM (RRID:SCR_007037) release 12.7771 (Whitfield-Gabrieli und Nieto-Castanon 2012; Nieto-Castanon und Whitfield-Gabrieli 2022) running on MATLAB v24.1.0.2628055 (R2024a) Update 4.

Functional and anatomical data were preprocessed and denoised using CONN (v22.v2407) and SPM12 (v7771) in MATLAB R2024a as follows:

- Realignment and Unwarping: Co-registration to the first scan using SPM's 6-parameter rigid-body transformation with b-spline interpolation and susceptibility distortion correction (Friston et al., 1995).
- Slice-Timing Correction: Sinc interpolation to a common mid-acquisition time (Nieto-Castanon, 2020d).
- Outlier Detection: Artifact Detection Toolbox (ART) flagged scans with framewise displacement >2 mm or global BOLD changes >9 SDs, creating a reference image from non-outlier scans.
- Normalization and Segmentation: Direct normalization to MNI space using SPM's unified algorithm with IXI-549 template, segmented into grey/white matter and CSF, resampled to 2 mm isotropic voxels (Ashburner & Friston, 2005).
- Smoothing: Gaussian kernel, 8 mm FWHM.
- Denoising: Regression of 5 aCompCor components each from white matter/CSF, 12 motion components (6 movement parameters and 6 1st-order derivatives), outlier scans (< 42 factors), and linear trends (2 components), followed by 0.008–0.09 Hz bandpass filtering (Hallquist et al. 2013; Nieto-Castanon 2020, 2022; Whitfield-Gabrieli und Nieto-Castanon 2012). Effective degrees of freedom: 657.7–670.7 ($M = 670.2$, $SD = 2.1$).

2.3.1. First-level analysis MVPA

For each seed voxel, we computed the correlation between its preprocessed BOLD time series and the time series of all other voxels in the brain (bivariate correlations, Fisher z-transformed). This whole-brain connectivity map was then entered into a subject-level singular value decomposition (SVD) to reduce dimensionality. We retained the first 64 components from the SVD, from which the 10 components explaining the most variance in connectivity patterns were selected to form the eigenpattern-score maps (Whitfield-Gabrieli und Nieto-Castanon 2012). Each eigenpattern-score map reflects the strength of a dominant whole-brain connectivity pattern for that seed voxel per subject and condition. All analyses used CONN's default gray-matter mask and preprocessing settings, with no additional masking or dimensionality reduction applied beyond the steps described.

2.3.2. Second-level analysis MVPA

The eigenpattern-score images from the first-level analysis served as dependent variables in a voxel-wise General Linear Model (GLM) to test for condition-specific differences in connectivity patterns. For each voxel, a separate GLM was estimated, incorporating the 10 eigenpattern-score maps per subject and condition as inputs, with multivariate parametric statistics, random effects across subjects, and sample covariance estimation across measurements (Nieto-Castanon, 2022).

The primary hypothesis was evaluated using an interaction contrast [-1 1 1 -1] applied to the conditions (Verum Pre, Verum Post, Sham Pre, Sham Post), which captures differential changes in connectivity patterns between Verum ([Post - Pre]) and Sham ([Post - Pre]) sessions. All 10 eigenpattern components were included, and an F-test assessed any significant multivariate effect across these components in the interaction contrast. Voxel-level inferences were thresholded at $p < 0.05$ (FDR-corrected); cluster-level inferences used Gaussian Random Field theory with family-wise FDR-corrected $p < 0.05$ (Nieto-Castanon, 2020a). Significant clusters were interpreted as hubs of interaction-driven pattern heterogeneity and used as seeds for exploratory post-hoc seed-to-voxel analyses.

2.3.3. Exploratory post-hoc seed-to-voxel analyses

The resulting clusters derived by the MVPA-analyses (Interaction effect) were used as seed ROIs to calculate a seed-to-voxel analysis to further explore the details of the connectivity patterns underpinning the Intervention (Matos et al. 2023; Arnold Anteraper et al. 2019). Threshold-Free Cluster Enhancement (TFCE) with a statistical threshold of $p < 0.05$ (FWE) was selected for the seed-to-voxel analysis due to its unique ability to detect both small, focal effects and large, distributed connectivity patterns without relying on arbitrary initial thresholds (Smith und Nichols 2009). For further information regarding the rationale for this approach see supplementary material (section Rationale for Statistical Thresholding and Correction Methods in fc-MVPA and Seed-to-Voxel Analyses)

The following post-hoc paired *t*-test contrasts for each significant fc-MVPA cluster as seed were used to explore the connectivity patterns driving the fc-MVPA interaction effect: Verum post > verum pre; Sham post > Sham pre.

2.4. Psychophysiological data recording, preprocessing and analysis

ECG and respiration were recorded during each 18-min fMRI measurement using the Philips Invivo Expression MR ECG and SpO₂ wireless modules (Gen-2) of the MRI system (Philips Medical Systems, Best, The Netherlands). Respiration was measured via an air cushion positioned at the navel and secured with a Velcro strap. ECG was recorded with four MR-compatible electrodes (Skintact FS-50C, Leonhard Lang GmbH, Innsbruck, Austria) placed according to the Philips MR manual (Fig. 2). Due to magneto-hydrodynamic (MHD) effects inside the MR scanner, R-peak detection in the ECG can be unreliable; therefore, a peripheral pulse unit (PPU) was additionally recorded via an SpO finger clip on the right index finger. All signals were sampled at 496 Hz.

Preprocessing and analysis were performed in the PhysioData Toolbox v0.6.3 (Sjak-Shie, 2022). Scanphys log files from the MRI console were imported directly into PhysioData. For each participant, data from the pre- and post-fMRI measurements of both verum and sham sessions yielded four time points per metric.

2.4.1. Heart rate and HRV

ECG preprocessing used the PhysioData ECG analyzer. Of the three recorded ECG vectors (V1, V2, average of V1+V2), the average was used by default, with V1 or V2 substituted when R-peak visibility was superior. A 10 Hz high-pass filter was applied to reduce MHD-related artifacts. R-peak detection from both ECG and PPU was visually inspected and manually corrected when necessary. Heart rate (HR) and heart rate variability (HRV) metrics were derived using the toolbox HRV analyzer with default settings. RMSSD (root mean square of successive differences, detrended) was used as the primary HRV measure, given its suitability for short-term recordings (Shaffer und Ginsberg 2017).

2.4.2. Respiration

Respiration data were processed with the PhysioData respiration analyzer, using default settings except for a minimum inhalation duration of 0.5 s. Inhalation/exhalation classifications were visually checked, and abnormal traces excluded. Mean breath duration (s) served as the respiration metric.

3. Statistical analyses

Statistical analyses for secondary endpoints were performed using SPSS 30 (version 30.0.0.0 (172), IBM Corp., Armonk, NY, USA). A statistical threshold of $p < 0.05$ (two-tailed) was chosen as criterion for statistical significance. Normality assumptions of the data were checked using visual inspections of Q-Q-plots, outlier plots and Kolmogorov-Smirnov tests. Depending on these assessments, parametric or non-parametric inference analyses were calculated.

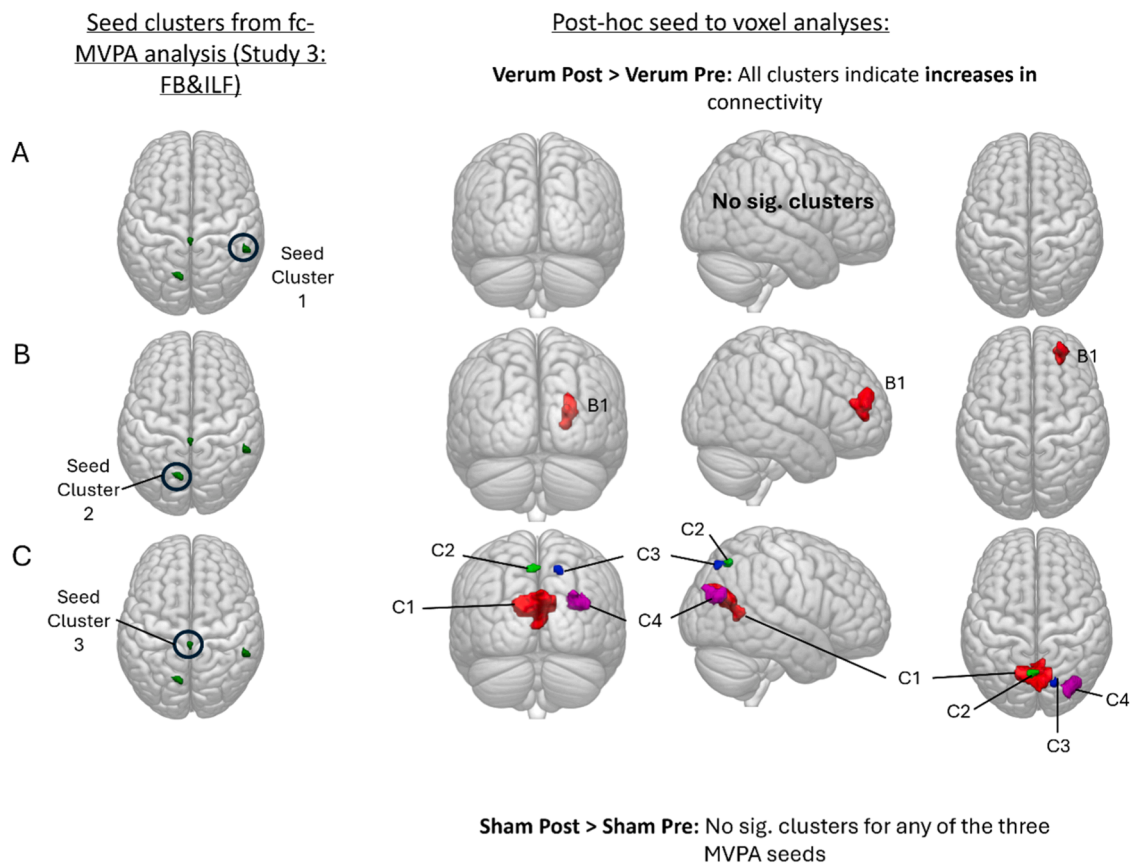


Fig. 2. Seed-to-voxel connectivity results from post-hoc analyses using seed clusters identified by the fc-MVPA interaction effect (Study 3: FB & ILF). Left panel Locations of three seed clusters derived from the fc-MVPA interaction analysis. Right panel: Results from seed-to-voxel analyses using these seed clusters. Each row (A–C) corresponds to one analysis using a specific seed cluster (green). Significant target clusters showing changes in connectivity with the seed are labeled and color-coded to distinguish separate clusters (colors are arbitrary and do not reflect direction of effect). Rows A–C display results from the Verum Post > Verum Pre contrast, showing increases in connectivity for all seed clusters. The comparison Sham post > Sham pre revealed no significant suprathreshold voxels and are thus not shown.

3.1. Psychophysiological data

Depending on the test for normality distribution, comparisons of the four timepoints (pre and post verum NFB; pre and post sham NFB) were either analyzed by means of a 2×2 factor repeated measures analysis of variance (ANOVA) with the factors intervention (Verum, Sham) and timepoint (pre or post), or by calculating the post-pre differences for the verum and sham condition and comparing them using a Wilcoxon signed-rank test.

3.2. Questionnaire data

Individual analyses of the NFB state questionnaire data were computed for each item. Items collected pre and post intervention were statistically analyzed by calculating post-pre differences for the verum and sham condition and comparing them using a Wilcoxon signed-rank test. For the ones only collected pre or post intervention, statistical significance was examined by a direct comparison of the means using a Wilcoxon signed-rank test.

4. Results

4.1. Analyzed datasets

As mentioned in the Materials & Methods section, we targeted a total 40 complete datasets for the analysis of the primary endpoint (fc-MVPA analysis) of each of the three independent studies (FB-Only, ILF-Only, FB&ILF). Table 1 summarizes the number of subjects included in the

study; number of datasets analyzed with explanations dataset exclusions. For the secondary outcomes, only the datasets included in the primary outcome analyses were considered, thus leading to a total of 40 included datasets.

4.2. Functional connectivity

The reporting of the functional connectivity analyses is structured to follow the approach described in the Materials & Methods section under “Functional Connectome Analysis”. At first, we describe the fc-MVPA results with respects to the interaction contrast. Significant effects were only found for the FB&ILF study.

As a next step, post-hoc seed-to-voxel analyses are performed using the identified fc-MVPA clusters from study FB&IF are used as seeds for further exploration.

In order to provide the reader with a comparative overview of the fundamental fc-MVPA patterns observed across studies, additional fc-MVPA analyses of the three studies with less stringent statistical thresholds ($p < 0.001$ uncorrected for voxel height and $p\text{-FDR} < 0.05$ corrected on cluster level) are reported as supplementary material. In the same vein,

4.2.1. fc-MVPA: FB&ILF

The fc-MVPA of the corrected interaction effect in the FB&ILF study revealed three clusters, primarily involving parietal, occipital, and cingulate regions. The first cluster was predominantly located in the right posterior supramarginal gyrus (pSMG r), highlighting the right-lateralized parietal involvement observed in the uncorrected analysis.

Table 1

Summary of number of included participants, analyzed datasets for primary/secondary endpoints and reasons for dataset exclusions.

Data analysis:	Datasets included/analyzed	Reasons for exclusions:
Study: FB-Only		
Primary Outcome:		
fMRI	44 / 40	2 datasets excluded due to strong movement, 2 datasets due to reconstruction error
Secondary Outcomes:		
HR/HRV	40 / 25	1 dataset excluded due to recording issues 14 datasets excluded due to insufficient data quality
Respiration	40 / 39	1 dataset excluded due to insufficient signal quality
Neurofeedback questionnaires:	40 / 40	
Study: ILF-Only		
Primary Outcome:		
fMRI	42 / 40	2 datasets excluded due to strong movement
Secondary Outcomes:		
HR/HRV	40 / 36	4 datasets excluded due to insufficient data quality
Respiration	40 / 36	4 datasets excluded due to insufficient data quality
Neurofeedback questionnaires:	40 / 40	
Study: FB&ILF		
Primary Outcome:		
fMRI	45 / 40	3 datasets excluded due to strong movement, 1 dataset due to reconstruction error 1 dataset due to problems during NFB application
Secondary Outcomes:		
HR/HRV	40 / 35	2 datasets excluded due to recording issues 3 datasets excluded due to insufficient data quality
Respiration	40 / 38	2 datasets excluded due to recording issues
Neurofeedback questionnaires:	40 / 40	

HR = Heart rate, HRV = Heart rate variability, fMRI = functional magnetic resonance imaging.

The second cluster included the precuneus cortex, accompanied by occipital regions such as the left supracalcarine cortex (SCC 1) and the left cuneal cortex (Cuneal 1). This cluster suggests that occipito-parietal regions remain relevant even after statistical correction, although in a more spatially restricted pattern.

The third cluster was centered on the posterior division of the cingulate gyrus (PC), with additional minor contributions from the left precentral gyrus (PreCG 1) and the precuneus cortex, indicating persistent involvement of midline and sensorimotor-related areas.

Illustrations and detailed characteristics of these clusters can be found in [Table 2](#).

4.2.2. Post-Hoc seed-to-voxel analyses: FB&ILF

This section summarizes exploratory post-hoc seed-to-voxel analyses using the three fc-MVPA-derived clusters (see [Table 3](#) and [Fig. 2](#)) as seeds to explore connectivity pattern alterations. Six analyses were conducted (three for Verum Post > Verum Pre, three for Sham Post > Sham Pre), with results thresholded at $p\text{-FWE} < 0.0083$ (Bonferroni-corrected for 6 comparisons, $0.05/6$) using threshold-free cluster enhancement (TFCE). Findings are detailed in [Table 3](#) and [Fig. 3](#). Additional non-Bonferroni-corrected analyses are reported in

Supplementary Results: Seed-to-Voxel Analysis.

Verum Post > Verum Pre:

No suprathreshold clusters were found for MVPA Cluster 1. For Cluster 2, Cluster B1 showed increased connectivity in the right dorso-lateral prefrontal cortex (frontal pole). For Cluster 3, four clusters showed enhanced connectivity: Cluster C1 centered on the precuneus cortex, extending along the medial parieto-occipital and calcarine fissures, including cuneal, intracalcarine, and supracalcarine cortices, posterior cingulate, lingual gyri, and cerebellum (vermis). Cluster C2 was located in the precuneus cortex, Cluster C3 in the right lateral occipital cortex (superior division), and Cluster C4 spanned the right lateral occipital cortex (superior division) and occipital pole.

Sham Post > Sham Pre:

No suprathreshold clusters were found for any MVPA clusters (1, 2, or 3).

4.3. Psychophysiological data

Heart rate, heart rate variability and respiration data recorded during the fMRI acquisitions are summarized in [Table 4](#).

4.3.1. Heart rate

2×2 rm-ANOVAs (condition \times time) revealed significant main-effect of time for all three studies (FB-Only: $F(1) = 8.006$, $p = 0.009$; ILF-Only: $F(1) = 60.025$, $p < 0.001$; FB&ILF: $f(1) = 50.188$, $p < 0.001$). However, no interaction effect was found for any of the three studies.

4.3.2. Respiration

For each of the three studies, effects of verum and sham NFB on respiratory cycle duration were investigated by pairwise comparisons of the post-pre differences in RMSSD using Wilcoxon signed-rank tests. The Wilcoxon tests revealed significantly lower post-pre differences after sham ($Z = -2.067$, $p = 0.039$) compared to verum. See [Fig. 3](#) for a visual representation of the described effect.

4.3.3. HRV

Analogous to the respiration data analysis, for each of the three studies, effects of verum and sham NFB on HRV were investigated by pairwise comparisons of the post-pre differences in RMSSD using Wilcoxon signed-rank tests. Only for the FB&ILF study a statistically significant effect was found ($Z = -2.621$, $p = 0.009$), which shows higher post-pre differences in sham compared to verum. See [Fig. 3](#) for a visual representation of the described effect.

4.3.4. Sensitivity analysis of respiration outliers on HRV

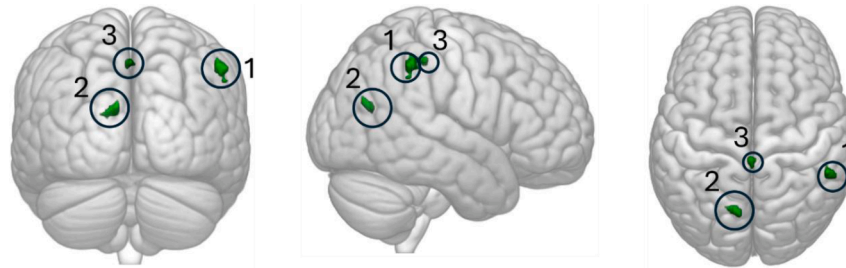
RMSSD, being used as a surrogate for parasympathetic activity, this metric is subject to influences of respiration via the physiological effect of respiratory sinus arrhythmia (RSA), although it is unclear to which extent ([Shaffer und Ginsberg 2017](#)). As for the FB&ILF study, effects of NFB condition (verum/sham) were found on post-pre differences in respiration and RMSSD, the question arises if the observed results for RMSSD are driven by extreme alterations in respiration data. In order to examine this possibility, extreme values in the post-pre differences in respiration were identified (see [Fig. 4](#)). A sensitivity analysis was subsequently done by 1) excluding the datasets of five study subjects exhibit extreme variations in respiratory frequency and by 2) repeating the Wilcoxon-tests. The removal of the identified subjects from the respiration dataset resulted in the loss of statistical significance ($Z = -1.291$, $p = 0.197$). However, the effects observed for RMSSD persisted ($Z = -2.293$, $p = 0.022$).

4.4. Questionnaire data

Items from the neurofeedback state questionnaire were compared between verum and sham conditions using Wilcoxon signed-rank tests. FB-Only study:

Table 2

Illustration, statistical characteristics and anatomical specification of the identified clusters from the fc-MVPA analysis for the FB&ILF study. The figure illustrates the three clusters which survived the statistical threshold of $p < 0.05$ (FDR) for voxel height and cluster level. The table reports MNI coordinates of peak voxels, cluster sizes, and associated significance levels (p-FWE, p-FDR, and uncorrected p-values) for both cluster size and peak intensity followed by the anatomical coverage overview including voxel count, percentage coverage, and corresponding brain regions.



Cluster	Coordinates (x/y/z)		Cluster size		size p-FWE	size p-FDR	size p-unc	peak p-FWE	peak p-unc
1	54	-42	44	43	0.000099	0.000774	0.000070	0.046695	0.000000
2	-10	-68	20	35	0.000338	0.001319	0.000240	0.036928	0.000000
3	0	-34	48	17	0.008140	0.021249	0.005795	0.029538	0.000000
Anatomical coverage									
Cluster	Voxel Count		% coverage		Region				
1	43		3 %		Supramarginal Gyrus posterior division right (pSMG r)				
2	24		1 %		Precuneous Cortex (Precuneous)				
	6		8 %		Supracalcarine Cortex left (SCC l)				
	2		0 %		Cuneal Cortex left (Cuneal l)				
	3		0 %		Not labeled				
3	7		0 %		Cingulate Gyrus posterior division (PC)				
	3		0 %		Precentral Gyrus left (PreCG l)				
	1		0 %		Precuneous Cortex (Precuneous)				
	6		0 %		Not labeled				

FWE = Familywise-error, FDR = False discovery rate, unc = uncorrected.

- **Controllability of feedback signals** (“1 = uncontrollable, 5 = controllable”): Higher controllability was reported during verum ($M = 2.97$, $SD = 1.33$) than sham ($M = 2.48$, $SD = 1.35$; $Z = -2.273$, $p = 0.023$).
- **Perception of signal origin** (“1 = I observed, 5 = came from me”): Participants reported a stronger impression that the signal came from them during verum ($M = 2.24$, $SD = 1.15$) than sham ($M = 1.73$, $SD = 0.63$; $Z = -2.973$, $p = 0.003$).

ILF-Only study:

- **Well-being** (“1 = high, 5 = low”): Participants reported better well-being during verum ($M = 1.68$, $SD = 0.62$) than sham ($M = 2.08$, $SD = 0.80$; $Z = -3.013$, $p = 0.003$).
- **Controllability of feedback signals**: Participants reported greater ease of regaining focus after distraction during verum ($M = 2.21$, $SD = 0.95$) than sham ($M = 2.60$, $SD = 1.03$; $Z = -2.381$, $p = 0.017$).
- **Sleepiness** (“1 = sleepy, 5 = awake”): Post-pre changes indicated a stronger shift towards sleepiness after verum ($M_{diff} = -1.08$, $SD = 1.44$) compared to sham ($M_{diff} = -0.55$, $SD = 1.36$; $Z = -2.554$, $p = 0.010$).
- **Calmness** (“1 = calm, 5 = nervous”): Post-pre changes differed significantly between conditions ($Z = -2.000$, $p = 0.045$), reflecting a slight shift towards nervousness after verum ($M_{diff} = 0.15$, $SD = 1.00$) and towards calmness after sham ($M_{diff} = -0.25$, $SD = 0.81$).

FB&ILF study:

- **Activity level** (“1 = increased, 5 = decreased”): Participants reported lower activity during verum ($M = 3.95$, $SD = 0.88$) than sham ($M = 3.61$, $SD = 0.86$; $Z = -1.980$, $p = 0.047$).
- **Perception of signal origin**: The impression that the signal came from them was stronger during verum ($M = 2.41$, $SD = 1.36$) than sham ($M = 1.93$, $SD = 0.85$; $Z = -2.058$, $p = 0.040$).

5. Discussion

A key gap in ILF-neurofeedback (ILF-NFB) research is the lack of understanding of how its two signal components, the classic frequency band (FB) and the infra-low frequency (ILF), individually and in combination affect brain neurophysiology. This limits the ability to determine whether both components are required to produce neurofeedback-specific effects, as defined in the framework proposed by Ros et al. (2020). Addressing this gap is a prerequisite to later evaluating whether the neuronal changes induced by ILF-NFB are relevant to clinical outcomes.

To close this gap, we conducted three randomized, sham-controlled, double-blind crossover studies that differed only in the composition of the real-time EEG-derived feedback signal (FB-Only, ILF-Only, FB&ILF). Because neural substrates of implicit ILF-NFB are not yet established and remain largely uncharacterized, we chose functional connectivity multivariate pattern analysis (fc-MVPA) as our main analytical tool. This hypothesis-free, voxel-wise approach can identify brain regions whose whole-brain connectivity patterns are altered by an intervention without requiring a priori ROI selection. The clusters identified in the fc-MVPA interaction contrast ([Post-Pre Verum] vs. [Post-Pre Sham]) were then examined in post-hoc seed-to-voxel analyses to map their specific network-level connections.

From the three studies, only FB&ILF, which simultaneously presented FB and ILF signal components in the feedback animations, produced clusters that survived our stringent statistical thresholds (both $p < 0.05$ [FDR] at voxel height and cluster level). Therefore, the discussion focuses on the FB&ILF study. For context, supplementary exploratory fc-MVPA analyses at a more lenient threshold (voxel height $p < 0.001$, uncorrected) showed no significant effects for ILF-Only, while FB-Only exhibited comparatively weaker right-hemispheric connectivity changes (Fig. S1, Tables S1a/b).

While these findings do not rule out the potential of FB-only or ILF-only protocols to induce neurophysiological changes under different

Table 3

Identified clusters from the seed-to-voxel analysis for the contrast verum post > verum pre, using cluster 2 and 3 from the fc-MVPA analysis as the seed region. MVPA seed 1 revealed no suprathreshold clusters. The table presents MNI coordinates of peak voxels, cluster size (voxel count), number of local peaks, TFCE values, and corresponding significance levels (p-FWE, p-FDR, and uncorrected p-values), followed by the anatomical coverage characteristics of each cluster. Results are thresholded at p-FWE < 0.0083 (Bonferroni-corrected for 6 comparisons [3 MVPA clusters x 2 contrasts]), based on the threshold-free cluster enhancement (TFCE) approach. Cluster labels were chosen according to Fig. 2.

Seed-to-voxel results with MVPA seed cluster 2									
Cluster	Coordinates (x/y/z)			Cluster size	Peaks	TFCE	peak p-FWE	peak p-FDR	peak p-unc
B1	26	44	14	351	2	1362.2	0.007	0.06748	0.000132
Anatomical Coverage									
Cluster	Voxel count			%-coverage	Region				
B1	272			3 %	FP r (Frontal Pole Right)				
	79			0 %	Not-labeled				
Seed-to-voxel results with MVPA seed cluster 3									
Cluster	Coordinates (x/y/z)			Cluster size	peaks	TFCE	peak p-FWE	peak p-FDR	peak p-unc
C1	-06	-66	+14	888	3	1853.82	0.001	0.003942	0.000004
C2	-04	-68	+48	47	1	1552.29	0.005	0.004519	0.000068
C3	+20	-76	+46	41	1	1538.75	0.006	0.004519	0.000071
C4	+36	-78	+16	315	1	1519.72	0.007	0.004519	0.000075
Anatomical Coverage									
Cluster	Voxel count			%-coverage	Region				
C1	565			10 %	Precuneus (Precuneus Cortex)				
	123			19 %	Cuneal r (Cuneal Cortex Right)				
	35			7 %	Cuneal l (Cuneal Cortex Left)				
	31			5 %	ICC l (Intracalcarine Cortex Left)				
	25			34 %	SCC l (Supracalcarine Cortex Left)				
	24			4 %	Ver45 (Vermis 4 5)				
	11			1 %	LG r (Lingual Gyrus Right)				
	7			5 %	SCC r (Supracalcarine Cortex Right)				
	6			1 %	ICC r (Intracalcarine Cortex Right)				
	5			0 %	LG l (Lingual Gyrus Left)				
	1			0 %	PC (Cingulate Gyrus, posterior division)				
	55			0 %	Not-labeled				
C2	47			1 %	Precuneus (Precuneus Cortex)				
C3	41			1 %	sLOC r (Lateral Occipital Cortex, superior division Right)				
C4	306			6 %	sLOC r (Lateral Occipital Cortex, superior division Right)				
	1			0 %	OP r (Occipital Pole Right)				
	8			0 %	Not-labeled				

FWE = Familywise-error, FDR = False discovery rate, unc = uncorrected.

conditions (e.g., higher sample sizes, repeated sessions, or clinical populations), the present results suggest that the concurrent presentation of both signal components yields more robust and spatially distributed effects. This may reflect additive or synergistic mechanisms that enhance network-level plasticity when both frequency domains are engaged simultaneously.

5.1. FB&ILF produced the only robust fc-MVPA interaction effects

Only the combined FB&ILF protocol, presenting both frequency-band and infra-low-frequency components simultaneously, elicited significant interaction effects in the fc-MVPA analysis. Three clusters survived rigorous correction (Table 2):

- Cluster 1: right posterior supramarginal gyrus
- Cluster 2: precuneus with parieto-occipital extensions
- Cluster 3: posterior cingulate cortex with minor precentral and precuneus contributions

Post-hoc seed-to-voxel analyses showed that only Cluster 2 and Cluster 3 exhibited significant connectivity increases after verum FB&ILF, none were detected in the sham condition (Fig. 2, Table 3).

Cluster 2 → right dorsolateral prefrontal cortex (rDLPFC)

The sole significant target for Cluster 2 was located in the right DLPFC/frontal pole (B1). The rDLPFC is implicated in executive control functions such as working memory (Barbey et al. 2013), cognitive flexibility (Borwick et al. 2020), planning (Kaller et al. 2011), and inhibition (Oldrati et al. 2016). Neurofeedback studies have linked modulation of rDLPFC activity to improved emotion regulation (Yu et al.

2021) and enhanced self-regulatory capacity (Sherwood et al. 2016). Increased coupling between the precuneus/occipital seed and rDLPFC may therefore reflect strengthened communication between internally oriented processing hubs and a prefrontal control region, potentially supporting more effective top-down regulation.

Cluster 3 → occipital and parieto-occipital targets

Cluster 3 demonstrated four significant target clusters (C1–C4) located in the parieto-occipital cortex. The largest (C1) spanned medial parieto-occipital/precuneus territory with extensions into calcarine regions, posterior cingulate, lingual gyri, and cerebellar vermis. The remaining targets included a smaller precuneus region (C2) and two right lateral occipital clusters (C3, C4), with C4 extending to the occipital pole. The precuneus is a high-centrality hub involved in visuo-spatial processing, visuomotor integration, and self-related cognition (Cavanna und Trimble 2006). Stronger connectivity between this region and occipital areas may indicate enhanced integration of visual information with internally generated cognitive representations, processes that could be relevant for adaptive network reconfiguration during ILF-NFB.

Cluster 1 → no suprathreshold targets

Although Cluster 1 reached significance in the fc-MVPA interaction contrast, it did not yield any suprathreshold seed-to-voxel targets. This absence parallels the lack of significant findings for the sham post > pre contrast across all seeds. When applying more lenient, but still frequently used, statistical thresholds without Bonferroni correction, both Cluster 1 in the verum post > pre contrast and the sham post > pre contrast yielded detectable connectivity alterations (see supplementary figure S3, S6, tables S3a/b and S6a/b). These exploratory results suggest that weaker or more spatially diffuse effects, possibly related to non-

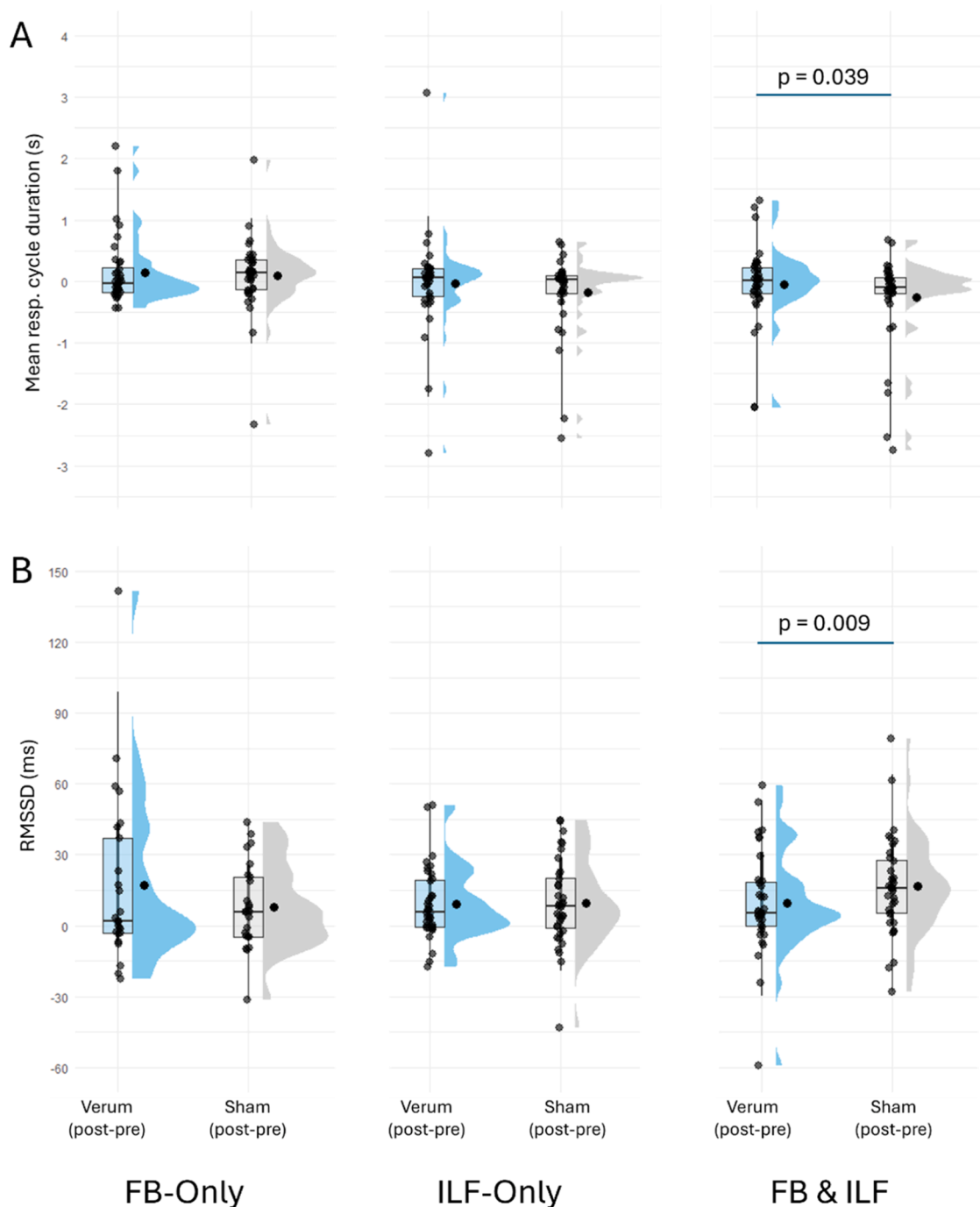


Fig. 3. Raincloud plots illustrating the post-pre differences of (A) mean respiration cycle duration and (B)RMSSD. These are plotted for the verum and sham conditions of each of the three studies (FB-Only, ILF-Only and FB&ILF). The graphs are composed of a density plot for visualization of the distribution, supplemented by visualization of the mean, and boxplot surrounded by scattered individual data points. Significant differences between verum and sham (conducted using Wilcoxon signed-rank tests) are indicated by blue lines with the corresponding p-values for the given comparisons.

specific factors such as repeated scanning or visual stimulus exposure, may be present but are not robust enough to survive the stringent correction applied in the main analysis. In addition, differences between what the two methods capture may contribute to this divergence: fc-MVPA identifies regions showing strong changes in the pattern of whole-brain connectivity, whereas seed-to-voxel focuses on changes in the magnitude of correlation with specific target regions. A cluster may therefore be significant in the multivariate pattern space without any single connection being strong enough to meet the conservative univariate thresholds. This reinforces the importance of interpreting post-

hoc seed-to-voxel findings within the context of the primary fc-MVPA results.

5.2. Relating FB&ILF connectivity changes to prior findings

Our results are partly in line with the findings reported by Dobrushina et al. (2020), who also investigated the impact of ILF-NFB combining FB and ILF signal components on brain connectivity in healthy volunteers. They reported increases in connectivity between areas of the salience and visual networks after verum ILF-NFB. However,

Table 4

Descriptive statistics (mean and standard deviation) of psychophysiology parameters measured during the pre and post fMRI scans from the FB-Only, ILF-Only and FB&ILF study.

	Verum				Sham			
	Pre		Post		Pre		Post	
	M	SD	M	SD	M	SD	M	SD
FB-Only:								
HR (BPM)	63.46	7.56	60.78	7.15	63.43	7.78	61.22	8.27
HRV (RMSSD [ms])	56.37	26.76	73.59	41.80	68.03	32.88	76.09	36.96
Mean Resp Cycle Dur (s):	3.79	0.75	3.92	1.09	3.80	0.86	3.89	0.88
ILF-Only:								
HR (BPM)	66.54	8.04	61.99	6.44	65.72	7.87	60.97	7.02
HRV (RMSSD [ms])	60.06	33.40	69.27	34.56	66.39	35.32	75.89	39.01
Mean Resp Cycle Dur (s):	3.86	0.85	3.83	0.85	4.08	1.33	3.79	0.64
FB&ILF:								
HR (BPM)	69.31	7.44	64.06	6.14	70.12	8.43	64.28	7.04
HRV (RMSSD [ms])	52.53	30.00	62.12	27.89	49.22	27.57	65.91	27.89
Mean Resp Cycle Dur (s):	3.93	1.41	3.89	1.08	3.87	1.15	3.60	0.68

HR = Heart Rate, HRV = Heart Rate Variability, Resp cycle dur = Respirator cycle duration (time between inhalation peaks), BPM = beats per minute, RMSSD = Root Mean Squares of Successive Differences, s = seconds, ms = milliseconds.

a direct comparison is complicated by differences in fMRI sequences, connectivity analysis methods, experimental designs (between-subjects vs. our within-subjects), and the type of animation used for feedback presentation.

Our study was conceived as exploratory basic research to isolate the specific impact of simultaneously applying FB and ILF signal components on healthy brain connectivity. Although robust alterations were observed, attributing these changes to specific neuronal or cognitive processes requires dedicated studies in which targeted aspects of ILF-NFB-mediated neuronal self-regulation are systematically modulated. Similarly, no direct conclusions can be drawn about clinical effects from our findings. Nevertheless, the reported connectivity changes may represent potential modes of action underlying clinical effects and should be examined in future work. For example, increased coupling between posterior cingulate/precuneus and occipital cortices, and between posterior midline/parieto-occipital cortex and right dlPFC, raises the hypothesis of altered top-down regulation that could influence cognitive flexibility. Experimental designs incorporating behavioral assessments could help test such relationships.

While ILF-NFB follows an implicit protocol without explicit strategy use, some of the same target regions highlighted in explicit neurofeedback paradigms (Sitaram et al. 2017) emerged in our FB&ILF findings. In explicit EEG- and fMRI-based protocols, the dlPFC is consistently engaged as part of the “control network,” supporting executive functions and top-down modulation. In our study, increased coupling between the precuneus/parieto-occipital cortex and the right dlPFC suggests that even without reinforcement learning or reward-based feedback, mere presentation of brain signals may be sufficient to facilitate aspects of top-down control. In contrast, we did not observe changes in reward-processing regions such as the anterior cingulate cortex or striatum, which are typically engaged in explicit protocols relying on reinforcement learning (Sitaram et al. 2017). This divergence is consistent with the implicit nature of ILF-NFB and suggests that its network effects may bypass classic reward circuits. Future research should investigate whether rDLPFC–occipital coupling plays a role in clinical outcomes and whether such effects represent a common pathway of neuroplasticity shared between explicit and implicit approaches.

The observed connectivity changes unfolded within minutes, at least persisting for the duration of the experiment. This rapid effect has also been observed in other neurofeedback studies (Altan et al. 2016;

Dobrushina et al. 2020). However, the temporal persistence of these effects should be examined in future research to assess their durability and potential clinical relevance. Unlike our single-session study, many clinical ILF-NFB protocols involve up to 40 sessions (Bazzana et al. 2022). If the identified connectivity patterns reflect potential mechanisms of clinical benefit, understanding how they interact with pathological network alterations and how they evolve across repeated sessions will be crucial. As Ros et al. (2020) note, the influence of non-specific factors on neurofeedback outcomes must also be considered. Systematic investigations of each signal component alone and in combination in clinical settings could inform optimization of ILF-NFB protocols for therapeutic use.

5.3. Psychophysiological effects of FB&ILF

In addition to functional connectivity, we measured breathing and heart rate–derived metrics to explore possible ILF-NFB effects on the autonomic nervous system (ANS) during fMRI recordings. The rationale was that if verum ILF-NFB fosters implicit self-regulation of the central nervous system, this could be reflected in ANS activity, possibly through top-down modulation. Heart rate variability (HRV) was indexed by the root mean square of successive differences (RMSSD), a widely used marker of parasympathetic activity (Berntson et al. 2016; Electrophysiology 1996; Shaffer und Ginsberg 2017). RMSSD is linked to respiratory sinus arrhythmia (RSA) which are systematic heart rate fluctuations during the breathing cycle (Grossman und Taylor 2007) and may be influenced by respiration rate, though the nature of this relationship remains uncertain (Shaffer and Ginsberg 2017). Therefore, respiratory frequency and heart rate were also analyzed.

Consistent with the imaging results, condition-specific alterations in RMSSD occurred only in the FB&ILF study. A non-parametric comparison of post–pre differences between verum and sham revealed a significantly greater RMSSD increase after sham FB&ILF. This effect was not attributable to heart rate, which decreased similarly in both conditions, as shown by the absence of an interaction effect. However, respiratory cycle duration showed an interaction effect, with more extreme post–pre changes (mainly shorter cycles, indicating faster breathing) in the sham condition. Sensitivity analysis excluding five participants with the most pronounced respiratory changes eliminated the respiration interaction but left the RMSSD effect intact. This supports the view that the RMSSD differences reflect distinct verum–sham impacts on parasympathetic

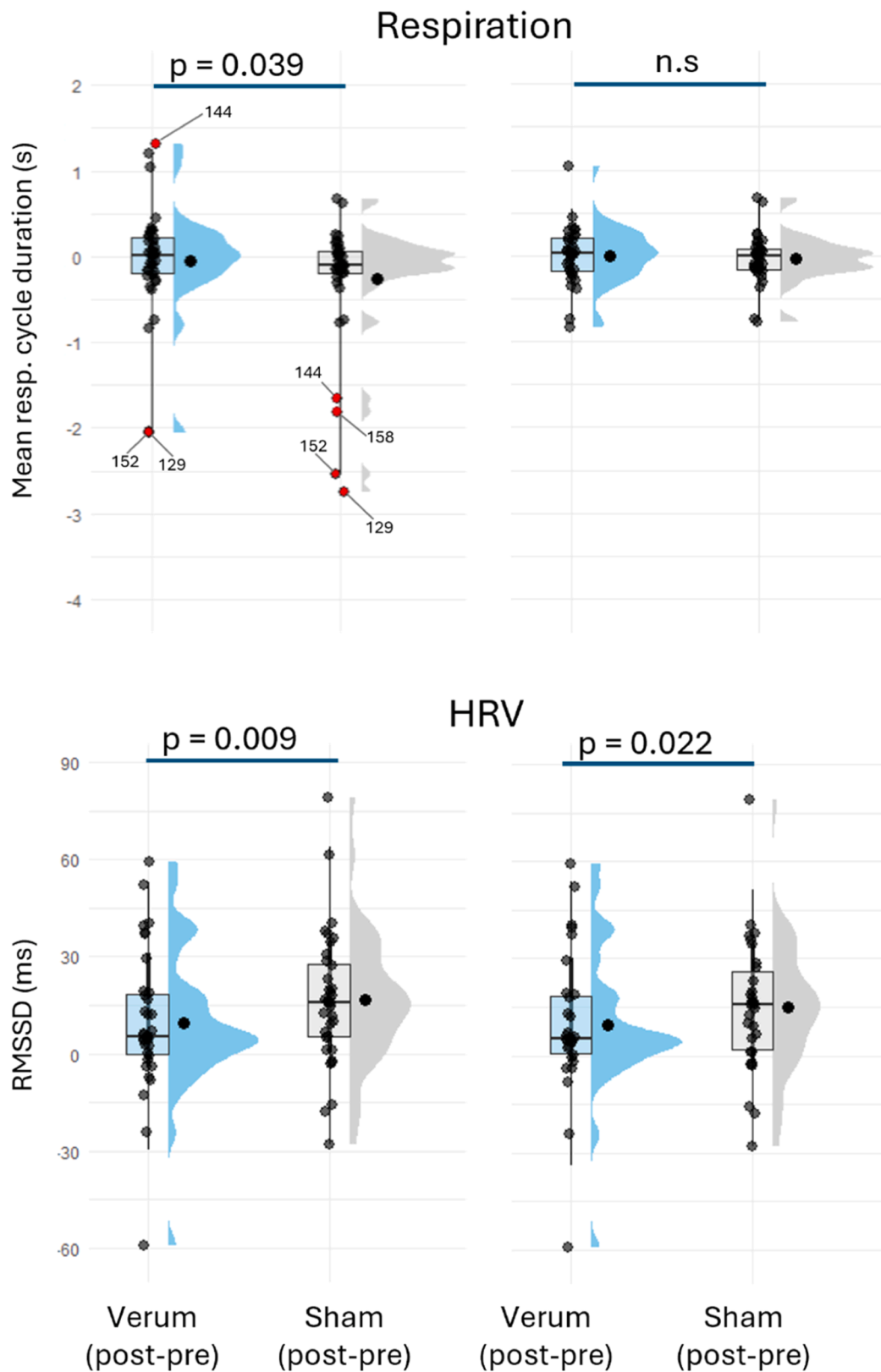


Fig. 4. Raincloud plots illustrating the post-pre differences of mean respiration cycle duration (row) and RMSSD (lower row) of the FB&ILF study before (left column) and after (right column) removal of outliers in the respiration data. This was done in the context of a sensitivity study to investigate the impact of extreme changes in respiration on the RMSSD analysis. The left plot in the upper row shows the five identified datasets (red dots, the number connected to the dots correspond to the subject ID) from the five subjects which exhibited strong differences in respiration. After removal, the RMSSD differences between verum and sham persisted, but not for the respiration data. Statistical significance between verum and sham (conducted using Wilcoxon signed-rank tests) is indicated by blue lines with the corresponding p-values for the given comparisons.

activity rather than being driven by respiration artifacts.

The mechanisms underlying these RMSSD effects remain unclear. This is, to our knowledge, the first study to examine short-term (single-session) ILF-NFB effects on the ANS in healthy volunteers. Neurofeedback state questionnaire results offered little explanation: in FB&ILF, verum was associated with higher perceived control over the feedback signal and lower perceived activity levels, but no significant verum–sham differences emerged for relaxation, happiness, boredom, sleepiness, or nervousness. One possibility is that post-verum fMRI sessions involved greater cognitive engagement linked to perceived control, but the questionnaires were administered immediately after NFB, not during the subsequent fMRI scan, so real-time states were not captured. Future work should incorporate in-scanner assessments of cognition, arousal, and well-being to clarify the relationship between ILF-NFB and ANS modulation.

Given the lack of meaningful differences in subjective ratings and the limited variability expected in a healthy, single-session sample, the neurofeedback state questionnaire appears to offer limited added value in this context. Future studies may benefit from using more sensitive or validated instruments, or from focusing on clinical populations where subjective effects may be more pronounced.

5.4. Limitations and future directions

Several limitations should be considered when interpreting these findings. First, the study used a single-session design in healthy volunteers, whereas clinical ILF-NFB protocols typically involve multi-session interventions, often with up to 40 sessions (Bazzana et al., 2022). The focal rather than widespread effects observed here after stringent correction may reflect the short duration of training in a healthy sample. Future studies should test whether repeated FB&ILF sessions produce more extensive or sustained connectivity changes and whether these translate into behavioral or symptomatic benefits.

Second, while the corrected results highlight specific couplings between posterior midline/parieto-occipital regions and right dorsolateral prefrontal cortex, and between posterior cingulate/precuneus and occipital areas, their functional relevance remains to be determined. Behavioral tasks could be used to assess whether these connections support cognitive flexibility, visuospatial integration, or other functions potentially relevant to clinical outcomes.

Third, we used a whole-head fc-MVPA approach to avoid a priori region or cluster selection. However, because fc-MVPA identifies regions based on changes in the *pattern* of whole-brain connectivity rather than the *strength* of individual connections, it may miss clusters that exhibit simple connectivity patterns but strong correlational changes. These are effects that could be detected with post-hoc seed-to-voxel analyses. Future studies may apply other approaches for whole-head connectivity characterization to identify potentially missed alterations and provide a more comprehensive view of neurofeedback-induced connectivity changes.

Fourth, the physiological findings, particularly the RMSSD effects, were intriguing but not mechanistically resolved, and we did not directly link them to the connectivity changes. Additional work is needed to determine whether FB&ILF-induced ANS modulation shares underlying mechanisms with the observed brain connectivity effects.

Fifth, as ILF-NFB is an implicit method without explicit performance metrics, we could not relate connectivity outcomes to regulation success. Objective EEG-based markers of ILF-NFB impact during training could help establish such links in future studies.

Sixth, the neurofeedback state questionnaire used here is not a validated instrument. While it provided exploratory insights into participants' perceptions and subjective states, its psychometric properties are unknown. Future studies should validate such questionnaires or employ standardized, validated tools to assess subjective experience during neurofeedback.

Finally, as Ros et al. (2020) emphasize, non-specific influences such

as placebo effects, expectation, and general engagement may contribute to neurofeedback outcomes. While our sham-controlled, within-subjects design aimed to minimize such influences, they cannot be fully excluded. Systematic evaluation of both signal-specific and non-specific contributions will be important for optimizing ILF-NFB protocols.

6. Conclusion

In this three-study project, robust, regionally specific alterations in functional brain connectivity after a single ILF-NFB session were observed only when FB and ILF signal components were presented simultaneously. In FB&ILF, but not FB-Only or ILF-Only, whole-head fc-MVPA followed by Bonferroni-corrected seed-to-voxel analyses revealed increased coupling between posterior midline/parieto-occipital regions and the right dorsolateral prefrontal cortex, and between posterior cingulate/precuneus and occipital areas. These findings suggest that combining both signals engages neural circuits more effectively than either alone and offer a basis for future research into potential mechanisms and their relevance in extended training protocols or clinical contexts.

Funding statement

The author(s) declare financial support was received for the research, authorship, and/or publication of this article. This study was funded by the Trauma Research Foundation. The funder was not involved in the study design, collection, analysis, interpretation of data, the writing of this article or the decision to submit it for publication. All authors declare no other competing interests.

Data and Code Availability

The datasets and analysis code used in this study are available from the corresponding author upon reasonable request.

Ethics statement

The study was approved and conducted in accordance with the regulations of the ethics committee of the Canton of Zurich (BASEC No 2018–00,550) and the Declaration of Helsinki. All participants provided their written informed consent to participate in the study. The study was preregistered on the clinicaltrials.gov database (NCT05711550)

Data Availability

The datasets used and/or analysed during the current study are available from the corresponding author on reasonable request.

CRediT authorship contribution statement

Nuno M.P. de Matos: Writing – review & editing, Writing – original draft, Visualization, Validation, Supervision, Software, Resources, Project administration, Methodology, Investigation, Funding acquisition, Formal analysis, Data curation, Conceptualization. **Philipp Stämpfli:** Writing – review & editing, Supervision, Resources, Project administration, Funding acquisition, Conceptualization. **Erich Seifritz:** Writing – review & editing, Resources, Funding acquisition. **Mike Brügger:** Writing – review & editing, Writing – original draft, Visualization, Validation, Supervision, Software, Resources, Project administration, Methodology, Investigation, Funding acquisition, Formal analysis, Data curation, Conceptualization.

Declaration of competing interest

The authors declare that the research was conducted in the absence of any commercial or financial relationships that could be construed as a potential conflict of interest.

Supplementary materials

Supplementary material associated with this article can be found, in the online version, at [doi:10.1016/j.neuroimage.2025.121647](https://doi.org/10.1016/j.neuroimage.2025.121647).

References

- Altan, Sümeyra, Berberoglu, Bercim, Canan, Sinan, Dane, Şenol, 2016. Effects of neurofeedback therapy in healthy young subjects. *CIM* 39 (6). <https://doi.org/10.25011/cim.v39i6.27496>. S. 27.
- Arnold Anteraper, Sheeba, Guell, Xavier, D'Mello, Anila, Joshi, Neha, Whitfield-Gabrieli, Susan, Joshi, Gagan, 2019. Disrupted cerebrotocerebellar intrinsic functional connectivity in young adults with high-functioning Autism spectrum disorder: a data-driven, whole-brain, high-temporal resolution functional Magnetic resonance imaging study. *Brain. Conn.* 9 (1). <https://doi.org/10.1089/brain.2018.0581>. S. 48–59.
- Barbey, Aron K., Koenigs, Michael, Grafman, Jordan, 2013. Dorsolateral prefrontal contributions to human working memory. *Cortex* 49 (5), 1195–1205. <https://doi.org/10.1016/j.cortex.2012.05.022>. S.
- Bazzana, Fabian, Finzi, Sarah, Fini, Di, Giulia, Veglia, Fabio, 2022. Infra-low frequency neurofeedback: a systematic mixed studies review. *Front. Hum. Neurosci.* 16, 920659. <https://doi.org/10.3389/fnhum.2022.920659>. S.
- Berntson, Gary G., Quigley, Karen S., Norman, Greg J., Lozano, David L., 2016. Cardiovascular psychophysiology. Editors: In: Cacioppo, John T., Tassinary und, Louis G., Gary, G. (Eds.), *Berntson (Hg.): Handbook of Psychophysiology*. Cambridge University Press (Cambridge Handbooks in Psychology), pp. 183–216. S.
- Borwick, Ciara, Lal, Reece, Lim, Lee Wei, Stagg, Charlotte J., Aquili, Luca, 2020. Dopamine depletion effects on cognitive flexibility as modulated by tDCS of the dlPFC. *Brain. Stimul.* 13 (1), 105–108. <https://doi.org/10.1016/j.brs.2019.08.016>. S.
- Britz, Juliane, van de Ville, Dimitri, Michel, Christoph M., 2010. BOLD correlates of EEG topography reveal resting-state network dynamics. *NeuroImage* 52 (4), 1162–1170. <https://doi.org/10.1016/j.neuroimage.2010.02.052>. S.
- Carlson, Judy, Ross, G. Webster, 2021. Neurofeedback impact on chronic headache, sleep, and attention disorders experienced by veterans with mild traumatic brain injury: a pilot study. *Biofeedback* 49 (1), 2–9. <https://doi.org/10.5298/1081-5937-49.01.01>. S.
- Cavanna, Andrea E., Trimble, Michael R., 2006. The precuneus: a review of its functional anatomy and behavioural correlates. *Brain: J. Neurol* 129 (Pt 3), 564–583. <https://doi.org/10.1093/brain/awl004>. S.
- Cho, Mi Kyung, Jang, Hwan Soo, Jeong, Sung-Hoon, Jang, Il-Sung, Choi, Byung-Ju, Lee, Maan-Gee T., 2008. Alpha neurofeedback improves the maintaining ability of alpha activity. *Neuroreport* 19 (3), 315–317. <https://doi.org/10.1097/WNR.0b013e3282f4f022>. S.
- Dobrushina, Olga R., Vlasova, Roza M., Rumshiskaya, Alena D., Litvinova, Liudmila D., Mershina, Elena A., Sinitsyn, Valentin E., Pechenkova, Ekaterina V., 2020. Modulation of intrinsic brain connectivity by implicit electroencephalographic neurofeedback. *Front. Hum. Neurosci.* 14, 192. <https://doi.org/10.3389/fnhum.2020.00192>. S.
- Electrophysiology, Task Force of the European Society of Cardiology the North A, 1996. Heart rate variability. *Circulation* 93 (5), 1043–1065. <https://doi.org/10.1161/01.CIR.93.5.1043>. S.
- Engelbregt, H.J., Keeser, D., van Eijk, L., Suiker, E.M., Eichhorn, D., Karch, S., et al., 2016. Short and long-term effects of sham-controlled prefrontal EEG-neurofeedback training in healthy subjects. *Clin. Neurophysiol.* 127 (4), 1931–1937. <https://doi.org/10.1016/j.clinph.2016.01.004>. S.
- Enriquez-Geppert, Stefanie, Huster, René J., Herrmann, Christoph S., 2017. EEG-neurofeedback as a tool to modulate cognition and behavior: a review tutorial. *Front. Hum. Neurosci.* 11, 51. <https://doi.org/10.3389/fnhum.2017.00051>. S.
- Gerge, Anna, 2020. A multifaceted case-vignette integrating neurofeedback and EMDR in the treatment of complex PTSD. *Eur. J. Trauma. Dissociat.* 4 (3), 100157. <https://doi.org/10.1016/j.ejtd.2020.100157>. S.
- Grin-Yatsenko, Vera, Othmer, Siegfried, Ponomarev, Valery, Evdokimov, Sergey, Konoplev, Yuri, Kropotov, Juri, 2018. Infra-low frequency neurofeedback in depression: three case studies. *NR* 5 (1), 30–42. <https://doi.org/10.15540/nr.5.1.30>. S.
- Grossman, Paul, Taylor, Edwin W., 2007. Toward understanding respiratory sinus arrhythmia: relations to cardiac vagal tone, evolution and biobehavioral functions. *Biol. Psychol.* 74 (2), 263–285. <https://doi.org/10.1016/j.biopsycho.2005.11.014>. S.
- Gruzelier, John H., 2014a. EEG-neurofeedback for optimising performance. I: a review of cognitive and affective outcome in healthy participants. *Neurosci. Biobehav. Rev.* 44, 124–141. <https://doi.org/10.1016/j.neubiorev.2013.09.015>. S.
- Gruzelier, John H., 2014b. EEG-neurofeedback for optimising performance. II: creativity, the performing arts and ecological validity. *Neurosci. Biobehav. Rev.* 44, 142–158. <https://doi.org/10.1016/j.neubiorev.2013.11.004>. S.
- Hallquist, Michael N., Hwang, Kai, Luna, Beatriz, 2013. The nuisance of nuisance regression: spectral misspecification in a common approach to resting-state fMRI preprocessing reintroduces noise and obscures functional connectivity. *NeuroImage* 82, 208–225. <https://doi.org/10.1016/j.neuroimage.2013.05.116>. S.
- Haus, Karl-Michael, Held, Carla, Kowalski, Axel, Krombholz, Andreas, Nowak, Manfred, Schneider, Edith, et al., 2020. Infra Low frequency (ILF-) neurofeedback (Hg.). In: Haus, Karl-Michael, Held, Carla, Kowalski, Axel, Krombholz, Andreas, Nowak, Manfred, Schneider, Edith, et al. (Eds.), *Praxisbuch Biofeedback und Neurofeedback*. Springer Berlin Heidelberg, Berlin, Heidelberg, pp. 91–112. S.
- Hoedlmoser, Kerstin, Pecherstorfer, Thomas, Gruber, Georg, Anderer, Peter, Doppelmayr, Michael, Klimesch, Wolfgang, Schabus, Manuel, 2008. Instrumental conditioning of human sensorimotor rhythm (12-15 Hz) and its impact on sleep as well as declarative learning. *Sleep* 31 (10), 1401–1408. S.
- Kaller, Christoph P., Rahm, Benjamin, Spreer, Joachim, Weiller, Cornelius, Unterrainer, Josef M., 2011. Dissociable contributions of left and right dorsolateral prefrontal cortex in planning. *Cereb. Cortex* 21 (2), 307–317. <https://doi.org/10.1093/cercor/bhq096>. S.
- Kamiya, Joe, 1968. Conscious control of brain waves. *Psychol. Today* (1), 5–60. S.
- Kamiya, Joe, 2011. The first communications about operant conditioning of the EEG. *J. Neurother.* 15 (1), 65–73. <https://doi.org/10.1080/10874208.2011.545764>. S.
- Kober, Silvia Erika, Schweiger, Daniela, Witte, Matthias, Reichert, Johanna Louise, Grieshofer, Peter, Neuper, Christa, Wood, Guilherme, 2015. Specific effects of EEG based neurofeedback training on memory functions in post-stroke victims. *J. Neuroeng. Rehabil.* 12, 107. <https://doi.org/10.1186/s12984-015-0105-6>. S.
- Legarda, Stella B., McMahon, Doreen, Othmer, Siegfried, Othmer, Sue, 2011. Clinical neurofeedback: case studies, proposed mechanism, and implications for pediatric neurology practice. *J. Child. Neurol.* 26 (8), 1045–1051. <https://doi.org/10.1177/0883073811405052>. S.
- Marzbani, Hengameh, Marateb, Hamid Reza, Mansourian, Marjan, 2016. Neurofeedback: a comprehensive review on system design, methodology and clinical applications. *Basic. Clin. Neurosci.* 7 (2), 143–158. <https://doi.org/10.15412/J.BCN.03070208>. S.
- Matos, Nuno M.P.de, Staempfli, Philipp, Seifritz, Erich, Preller, Katrin, Bruegger, Mike, 2023. Investigating functional brain connectivity patterns associated with two hypnotic states. *Front. Hum. Neurosci.* 17, 1286336. <https://doi.org/10.3389/fnhum.2023.1286336>. S.
- Murta, Teresa, Leite, Marco, Carmichael, David W., Figueiredo, Patrícia, Lemieux, Louis, 2015. Electrophysiological correlates of the BOLD signal for EEG-informed fMRI. *Hum. Brain. Mapp.* 36 (1), 391–414. <https://doi.org/10.1002/hbm.22623>. S.
- Nieto-Castanon, Alfonso, 2020. *Handbook of Functional Connectivity Magnetic Resonance Imaging methods in CONN*. Hilbert Press.
- Nieto-Castanon, Alfonso, 2022. Brain-wide connectome inferences using functional connectivity MultiVariate Pattern analyses (fc-MVPA). *PLoS. Comput. Biol* 18 (11), e1010634. <https://doi.org/10.1371/journal.pcbi.1010634>. S.
- Nieto-Castanon, Alfonso, Whitfield-Gabrieli, Susan, 2022. *CONN Functional Connectivity toolbox: RRID SCR_009550*, Release 22. Hilbert Press.
- Oldrati, Viola, Patricelli, Jessica, Colombo, Barbara, Antonietti, Alessandro, 2016. The role of dorsolateral prefrontal cortex in inhibition mechanism: a study on cognitive reflection test and similar tasks through neuromodulation. *Neuropsychologia* 91, 499–508. <https://doi.org/10.1016/j.neuropsychologia.2016.09.010>. S.
- Omejc, Nina, Rojc, Bojan, Battaglini, Piero Paolo, Marusic, Uros, 2019. Review of the therapeutic neurofeedback method using electroencephalography: EEG neurofeedback. *Bosn. J. Basic. Med. Sci.* 19 (3), 213–220. <https://doi.org/10.17305/bjbm.2018.3785>. S.
- Othmer, Siegfried, 2020. *History of neurofeedback*. Restoring. *Brain* 23–55.
- Othmer, Siegfried, Othmer, Sue, Legarda, Stella B., 2011. *Clinical neurofeedback: training brain behavior*. *Treat. Strateg. - Pediatr. Neurol. Psychiatry* 2 (1), 67–73. S.
- Othmer, Siegfried, Othmer, Susan F., Kaiser, David A., Putman, John, 2013. Endogenous neuromodulation at infralow frequencies. *Semin. Pediatr. Neurol.* 20 (4), 246–257. <https://doi.org/10.1016/j.spen.2013.10.006>. S.
- Renton, Tian, Tibbles, Alana, Topolovec-Vranic, Jane, 2017. Neurofeedback as a form of cognitive rehabilitation therapy following stroke: a systematic review. *PLoS. ONE* 12 (5), e0177290. <https://doi.org/10.1371/journal.pone.0177290>. S.
- Ros, Tomas, Enriquez-Geppert, Stefanie, Zotev, Vadim, Young, Kymberly D., Wood, Guilherme, Whitfield-Gabrieli, Susan, et al., 2020. Consensus on the reporting and experimental design of clinical and cognitive-behavioural neurofeedback studies (CRED-nf checklist). *J. Neurol.* 143 (6), 1674–1685. <https://doi.org/10.1093/brain/awaa009>. S.
- Scheeringa, René, Fries, Pascal, Petersson, Karl-Magnus, Oostenveld, Robert, Grothe, Iris, Norris, David G., et al., 2011. Neuronal dynamics underlying high- and low-frequency EEG oscillations contribute independently to the human BOLD signal. *Neuron* 69 (3), 572–583. <https://doi.org/10.1016/j.neuron.2010.11.044>. S.
- Schmidt, Casper, 2024. The potential of infra-low frequency neurofeedback training in peak performance: the first double-blinded placebo-controlled longitudinal study in healthy adults. *J. Psychiatr. Res.* 175, 280–286. <https://doi.org/10.1016/j.jpsychires.2024.04.035>. S.
- Schneider, Horst; Riederle, Jennifer; Seuss, Sigrid (2022): Therapeutic effect of infra-low-frequency neurofeedback training on children and adolescents with ADHD. In: Vahid Asadpour (Hg.): *Brain-Computer Interface, Bd. 9: IntechOpen (Artificial Intelligence)*, 9).
- Shaffer, Fred, Ginsberg, J.P., 2017. An overview of heart rate variability metrics and norms. *Front. Public. Health* 5, 258. <https://doi.org/10.3389/fpubh.2017.00258>. S.
- Sherlin, Leslie H., Arns, Martijn, Lubar, Joel, Heinrich, Hartmut, Kerson, Cynthia, Strehl, Ute, Sterman, M. Barry, 2011. Neurofeedback and basic learning theory: implications for research and practice. *J. Neurother.* 15 (4), 292–304. <https://doi.org/10.1080/10874208.2011.623089>. S.
- Sherwood, Matthew S., Kane, Jessica H., Weisend, Michael P., Parker, Jason G., 2016. Enhanced control of dorsolateral prefrontal cortex neurophysiology with real-time functional magnetic resonance imaging (rt-fMRI) neurofeedback training and working memory practice. *NeuroImage* 124 (Pt A), 214–223. <https://doi.org/10.1016/j.neuroimage.2015.08.074>. S.
- Sitaram, Ranganatha, Ros, Tomas, Stoeckel, Luke, Haller, Sven, Scharnowski, Frank, Lewis-Peacock, Jarrod, et al., 2017. Closed-loop brain training: the science of

- neurofeedback. *Nat. Rev. Neurosci.* 18 (2), 86–100. <https://doi.org/10.1038/nrn.2016.164>. S.
- Smith, Stephen M., Nichols, Thomas E., 2009. Threshold-free cluster enhancement: addressing problems of smoothing, threshold dependence and localisation in cluster inference. *NeuroImage* 44 (1), 83–98. <https://doi.org/10.1016/j.neuroimage.2008.03.061>. S.
- van der Kolk, Bessel A., Hodgdon, Hilary, Gapen, Mark, Musicaro, Regina, Suvak, Michael K., Hamlin, Ed, Spinazzola, Joseph, 2016. A randomized controlled study of neurofeedback for chronic PTSD. *PloS. One* 11 (12), e0166752. <https://doi.org/10.1371/journal.pone.0166752>.
- van der Kolk, Bessel A., Hodgdon, Hilary, Gapen, Mark, Musicaro, Regina, Suvak, Michael K., Hamlin, Ed, Spinazzola, Joseph, 2019. Correction: a randomized controlled study of neurofeedback for chronic PTSD. *PloS. One* 14 (4), e0215940. <https://doi.org/10.1371/journal.pone.0215940>.
- Whitfield-Gabrieli, Susan, Nieto-Castanon, Alfonso, 2012. Conn: a functional connectivity toolbox for correlated and anticorrelated brain networks. *Brain. Conn.* 2 (3), 125–141. <https://doi.org/10.1089/brain.2012.0073>. S.
- Wyrwicka, Wanda, Serman, Maurice B., 1968. Instrumental conditioning of sensorimotor cortex EEG spindles in the waking cat. *Physiol. Behav.* 3 (5), 703–707. [https://doi.org/10.1016/0031-9384\(68\)90139-X](https://doi.org/10.1016/0031-9384(68)90139-X). S.
- Yu, Linlin, Long, Quanshan, Tang, Yancheng, Yin, Shouhang, Chen, Zijun, Zhu, Chaozhe, Chen, Antao, 2021. Improving emotion regulation through real-time neurofeedback training on the right dorsolateral prefrontal cortex: evidence from behavioral and brain network analyses. *Front. Hum. Neurosci.* 15, 620342. <https://doi.org/10.3389/fnhum.2021.620342>. S.
- Zuberer, Agnieszka, Brandeis, Daniel, Drechsler, Renate, 2015. Are treatment effects of neurofeedback training in children with ADHD related to the successful regulation of brain activity? A review on the learning of regulation of brain activity and a contribution to the discussion on specificity. *Front. Hum. Neurosci.* 9, 135. <https://doi.org/10.3389/fnhum.2015.00135>. S.